Using Network Science to Evaluate ~~Vulnerability of Landslides~~ Landslide Hazards on Big Sur Coast, California, USA

Vrinda D. Desai[1,2], Alexander L. Handwerger[3,4], and Karen E. Daniels[1]

[1]Physics Department, North Carolina State University, Raleigh, NC, USA
[2]North Carolina Institute for Climate Studies, Asheville, NC, USA
[3]Joint Institute for Regional Earth System Science and Engineering, University of California Los Angeles, Los Angeles, CA, USA
[4]Jet Propulsion Laboratory, California Institute of Technology, Pasadena, CA, USA

Correspondence: Vrinda D. Desai (vddesai@ncsu.edu)

Abstract. Landslide events, ranging from slips to catastrophic failures, pose significant challenges for prediction. This study employs a physically inspired framework to assess landslide ~~vulnerability~~ hazard at a regional scale (Big Sur Coast, California). Our approach integrates techniques from the study of complex systems with multivariate statistical analysis to identify areas ~~vulnerable to landslide events~~prone to landslide hazards. We successfully apply a technique originally developed on the 2017 Mud Creek landslide and refine our statistical metrics to characterize landslide ~~vulnerability~~ hazard within a larger geographical area. Our method is compared against factors such as landslide location, slope, displacement, precipitation, and InSAR coherence using multivariate statistical analysis. Our network analyses, which ~~provides a natural way to incorporate~~ incorporates spatiotemporal dynamics, perform better as a monitoring technique than traditional methods. This approach has potential for real-time monitoring and evaluating landslide ~~vulnerability~~ hazard across multiple sites.

1 Introduction

With climate change leading to extreme weather conditions, such as heavy precipitation, there is an increased global danger of landslide hazards (Kirschbaum et al., 2020). One of the biggest challenges in real-time landslide hazard assessment is identifying and quantifying ~~landslide event vulnerability~~ the likelihood of landslide events within a geographical area ~~(Palmer, 2017),~~ (Hungr et al., 2014; Palmer, 2017) due to the inherent variability of hillslopes presenting non-uniform spatiotemporal dynamics (Lacroix et al., 2020; Glastonbury and Fell, 2008).

On the coast of California, landslides are abundant due to mechanically weak rocks, active uplift, and high seasonal precipitation, all of which contribute to general instability throughout the area. Hundreds of landslides have been identified as precipitation-induced by exploring the relationship between rainfall and landslide velocity (Handwerger et al., 2022; Scheingross et al., 2013; Bennett et al., 2016; Handwerger et al., 2019; Young, 2015; Booth et al., 2020; Wills et al., 2005; Jones et al., 2019; California Department of Conservation, 2023). As water infiltrates the ground, the water table rises, leading to an increase in pore-water pressure. This rise in pore-water pressure reduces the effective normal stress (difference between normal stress and pore-water pressure), which in turn decreases the frictional strength of the hillslope. This instability can lead to rapid

mass movement of material (rock, earth, debris) down the hillslope, defined as a *landslide event*. Identifying areas that are at immediate risk can help focus resources on the analysis, prevention, and risk reduction of these landslides.

In the winter of 2022-2023 (W22-3), the Big Sur Coast witnessed four landslide events ~~, three of which are~~ that occurred deeper than 1 m below the surface soil; and three of the four events were recorded by the California Geological Survey and the U.S. Geological Survey ~~. In Jan 2023, Paul's Slide reactivated, resulting in a shallow acceleration, with some of the landslide surface engulfing Highway 1 (Drabinski and Bertola, 2023a). Additionally, there were three other landslide events that occurred in the spring:~~ California Department of Conservation (2023) but were not catastrophic. These three landslide events – Dani Creek Slide (Mar 2023), Mill Creek (Jan 2023), and Gilbert's Slide (Mar 2023) (Drabinski and Bertola, 2023b) ~~.~~ – have not yet been studied to determine the specific landslide processes involved. The fourth landslide event occured in Jan 2023. Paul's Slide, a deep slow-moving landslide, reactivated, resulting in a shallow acceleration, with some of the landslide surface engulfing Highway 1 (Drabinski and Bertola, 2023a).

In this study, we ~~employ~~ apply network science techniques ~~,~~ – commonly used for studying complex systems ~~, to identify dynamic patterns in both~~ – to identify patterns that evolve over space and time. These techniques have been applied across a broad range of physical, biological, and social contexts (Barrat et al., 2008; Nguyen et al., 2019; Newman, 2010), including the study of granular and disordered materials (Bassett et al. 2011; Kivela et al. 2014; Mucha et al. 2010; Papadopoulos et al. 2016; Porter and Gleeson 2016; Nabizadeh et al. 2022; Berthier et al. 2019; Nguyen et al. 2019) .

The material beneath a hillslope consists of individual grains. Building on the success of network science in characterizing the behavior of granular systems, we previously developed a method to mathematically describe this type of hillslope through spatiotemporal relationships (Desai et al., 2023). In our approach, the hillslope is described as a set of geospatial points (nodes) connected by lines (edges), where each edge encodes measurable information about the relationship between nodes. In the context of landslides and this study, such information is derived from remote sensing observations.

The objective of this paper is to integrate ~~these techniques~~ the techniques developed in (Desai et al., 2023) with statistical analyses to classify geographical regions ~~into two categories:~~ as *stable* ~~and~~ or ~~*vulnerable*~~*hazard-prone* ~~. A region is considered vulnerable if it is likely to experience~~ based on the likelihood of a landslide event.

~~Such network science techniques have already been developed~~ We first tested these network techniques on Mud Creek, a slow-moving landslide on the Big Sur Coast that experienced a landslide event on 20 May 2017. ~~Desai et al. (2023) uses~~ In our earlier study, Desai et al. (2023), we used multilayer networks (Papadopoulos et al., 2016; Porter and Gleeson, 2016) and community detection ~~techniques~~ methods (Mucha et al., 2010; Porter et al., 2009) to retrospectively identify Mud Creek's location pre-failure and detect the transition from creeping to catastrophic failure.

In this paper, we ~~apply the same methods to~~ extend these methods across a broader section of the Big Sur Coast, shown in Fig. 1[a], using velocity from Interferometric Synthetic Aperture Radar (InSAR) time series and slope from a Digital Elevation Model (DEM). We ~~compare the results from implementing network science techniques~~ evaluate the effectiveness of the network-based approach by comparing it to multivariate analysis using physical ~~information~~ – variables: topography, ground surface deformation, precipitation, and satellite coherence~~– to evaluate the performance of network science techniques~~.

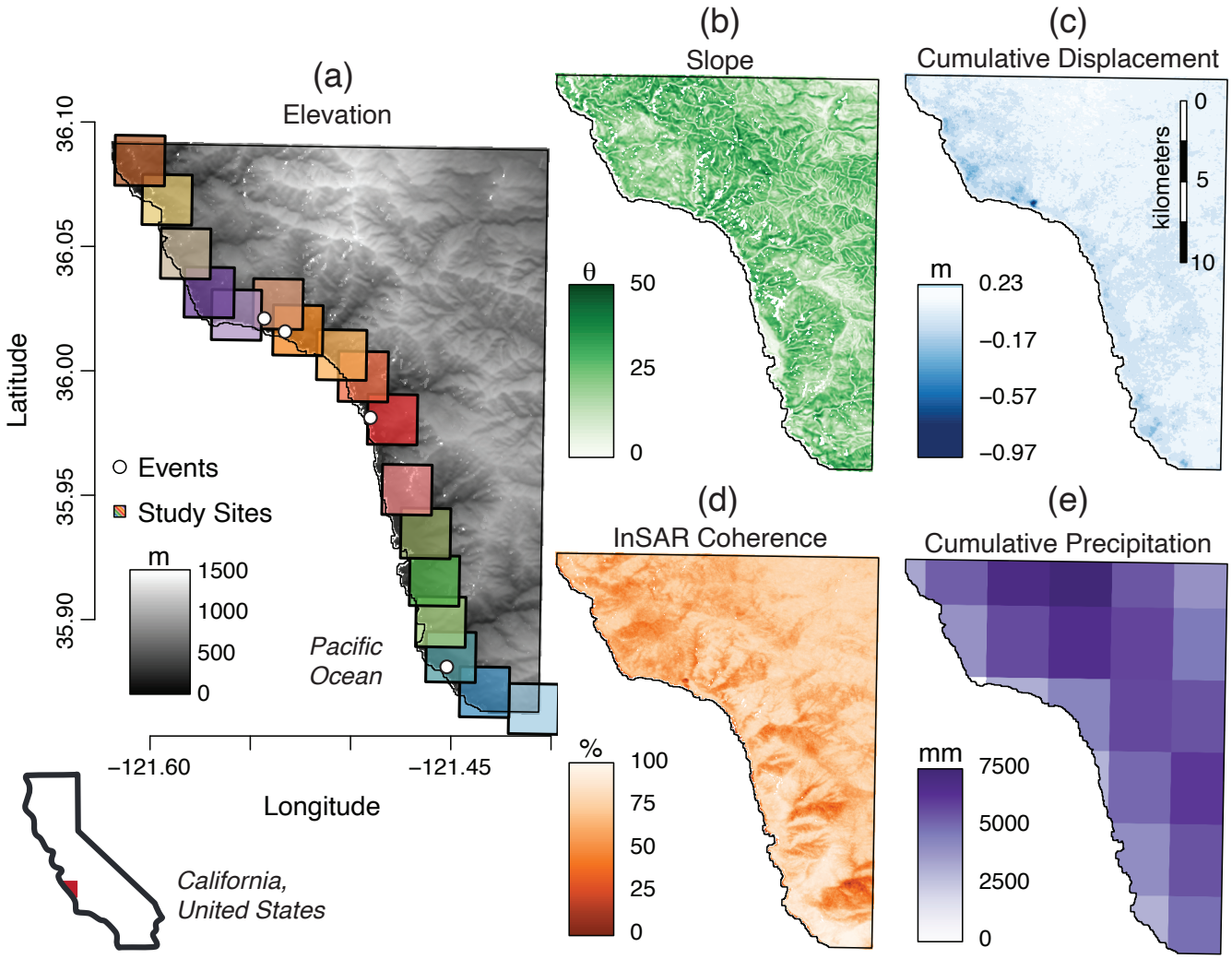

Figure 1. Regional scale maps of study area. (a) Digital elevation model of the study area. ~~44 active slow-moving landslides (grey polygons).~~ The 4 recorded landslide events by USGS and CA are shown as white dots. The black outlined boxes are the 17 sub-regions we used in this analysis. (b) Topographic slope angle (degrees). (c) Cumulative displacement from Sentinel-1 InSAR from Nov 2015 to ~~Nov~~ Dec 2022. (d) InSAR temporal coherence map. (e) Accumulated precipitation from PRISM from 1 Nov 2015 to 30 Nov 2022.

2 Data

We used ground surface deformation, topographic characteristics, and precipitation, which are commonly used in landslide ~~vulnerability~~ hazard maps and forecasting. We also include InSAR temporal coherence as a variable to measure satellite reliability. The following sections discuss these variables.

2.1 Study Area~~& LandslidesWe used a five-year time-averaged InSAR velocity map from Copernicus Sentinel-1 data, combined with digital elevation models (DEMs), Google Earth imagery, and published landslide inventories, to identify 44 active landslides along the coast of California using methods similar to those described in Handwerger et al. (2022). Of these 44 landslides, 14 were previously reported by Handwerger et al. (2022). These active slow-moving landslides have localized deformation with higher than average velocity compared to the study area. From this set, we identified 44 *active landslides* on the Big Sur Coast using a five-year InSAR velocity, shown in Fig. 1[a]. Only one of these experienced a deep-seated catastrophic failure: Mud Creek, which failed on 20 May 2017. Another prominent slow-moving landslide in this collection is Paul's Slide which has experienced many landslide events (accelerations), resulting in multiple roadblocks and recent landslide activity on 15 Jan 2023. We explore the temporal dynamics from 20 Nov 2015 to 19 Nov 2022, a few months before the four landslide events, to observe how our methods performed in classifying the sub-regions. The study area, the~~

The Big Sur Coast ~~,~~is divided into 17 sub-regions of similar size, roughly 5 km^2, and shown in Fig. 1[a]. This allows for ~~an~~ the application of the technique on more varied terrain containing both stable and unstable hillslopes (see discussion in §5.1), as well as ~~testing this~~ for testing the method as a prototype of how ~~the technique might work~~ this technique might be used in a monitoring context.

2.2 ~~Reported or Identified Landslide Events~~

~~The U.S. Geological Survey (Jones et al., 2019) and the California Geological Survey (California Department of Conservation, 2023) have reported and identified landslide events, compiling these into databases gathered from various local, state, and federal agencies. Although these databases are not exhaustive, they encompass shallow landslides, slow-moving landslide activity, rockfalls, and debris flows. The four landslide events of W22-3, represented as white points in Fig. 1[a], are located from north to south at Dani Creek Slide, Paul's Slide, Mill Creek, and Gilbert's Slide. Each of these landslide events involved seasonally-related mass downslope movements of hillslope material, with varying amounts of material removed during the clean-up process. Dani Creek Slide, Mill Creek, and Gilbert's Slide each resulted in the removal of roughly 23,000 cubic meters of material during repairs. In contrast, Paul's Slide, a notably slow-moving landslide that reactivated in Jan 2023, underwent over a year of repairs, during which approximately 385,000 cubic meters of material was removed (Drabinski and Bertola, 2023a, b, c)~~ .

2.2 Topography

We used the Copernicus Digital Elevation Model (DEM) (Copernicus, 2021), which provides elevation data at $(40 \times 40)\ \mathrm{m}^2$ resolution on a temporal interval of 6 or 12 days (corresponding to Sentinel-1 passes) and is shown in Fig. 1[a], to calculate the slope of each gridded cell within the study area, as depicted in Fig. 1[b]. We write the elevation field as $h(\boldsymbol{r})$, where $\boldsymbol{r} = (x, y)$ represents the position in UTM coordinates.

2.3 Ground Surface Deformation

We processed the Sentinel-1 InSAR data using the Alaska Satellite Facility's (ASF) On-Demand InSAR processing HyP3 platform (Hogenson et al., 2020). ASF's On-Demand InSAR tool constructs interferograms using the GAMMA software. The InSAR data are inverted to time series using the Miami InSAR Time-series software in Python (MintPy) software (Yunjun et al., 2019). We processed data on descending track 42 using two looks in azimuth and ten looks in range. Spanning from 20 Nov 2015 to ~~19 Nov~~ 01 Dec 2022, the dataset comprises 279 time slices at a resolution of (40×40) m^2 per grid cell, covering the study area of the Big Sur Coast. From the Sentinel-1 data, we utilized the displacement time series and a temporal coherence map in our analysis.

Each InSAR ~~snapshot~~ image provides line-of-sight displacement, indicating motion either towards or away from the satellite. Cumulative displacement, calculated as the difference between the last time slice on ~~19 Nov~~ 01 Dec 2022 and the first time slice on 20 Nov 2015, shows landslide activity over the seven years (as shown in Fig. 1[c]). Additionally, we computed the mean and maximum cumulative displacement values of each sub-region for use in multivariate analysis.

To analyze the motion of landslides for use in the network science techniques, we calculated the velocity for each InSAR ~~snapshot~~ image t as $v(x,y,t) = \frac{\Delta u(x,y)}{\Delta t}$, where Δu represents the relative displacement between pairs of adjacent snapshots and Δt denotes the time interval between any two consecutive snapshots. Due to the noise introduced by taking derivatives of the InSAR displacement data, we apply a 3×3 cell Gaussian kernel to smooth the data.

The temporal coherence map (Fig. 1[d]) measures the reliability of the InSAR displacement time series inversion. Pixels with coherence values below 65% were masked from the displacement maps. Low coherence values can occur due to a number of factors, including obscured or significant deformation (Fletcher et al., 2007; Yunjun et al., 2019). The applied mask excludes approximately 1.7% of the total area, with an average exclusion of 4.8% within each sub-region.

2.4 Precipitation

The Parameter Elevation Regressions on Independent Slopes Model (PRISM) database provides precipitation data modeled on a 4×4 km^2 grid cell resolution using station data and climate models (Oregon State Univeristy, 2015). We selected PRISM due to its performance in mountainous and coastal areas of the western United States and because there are no station data within the study area (Daly et al., 2008). The precipitation datasets span from 1 Nov 2015 to 30 Nov 2022 with daily maps, and we computed cumulative precipitation by summing over the entire period (as shown in Fig. 1[e]), with the mean precipitation calculated for each sub-region.

2.5 Reported or Identified Landslide Events

The U.S. Geological Survey (Jones et al., 2019) and the California Geological Survey (California Department of Conservation, 2023) have reported and identified landslide events, compiling these into the Reported California Landslides Database gathered from various local, state, and federal agencies. Although this database is not exhaustive, the entries encompass shallow landslides, slow-moving landslide activity, rockfalls, and debris flows. The four landslide events of W22-3, represented as white points

in Fig. 1[a], are located from north to south at Dani Creek Slide, Paul's Slide, Mill Creek, and Gilbert's Slide. Each of these landslide events involved seasonally-related mass downslope movements of hillslope material, with varying amounts of material removed during the clean-up process. Dani Creek Slide, Mill Creek, and Gilbert's Slide each resulted in the removal of roughly 23,000 cubic meters of material during repairs. In contrast, Paul's Slide, a notably slow-moving landslide that reactivated in Jan 2023, underwent over a year of repairs, during which approximately 385,000 cubic meters of material was removed (Drabinski and Bertola, 2023a, b, c).

3 ~~Network Science~~ Methods

3.1 Network Science

To classify sub-regions as ~~*vulnerable*~~*hazard-prone*, we used multilayer networks (Kivela et al., 2014; Porter and Gleeson, 2016; Papadopoulos et al., 2016; Bassett et al., 2011) to couple the temporally-resolved kinematics (velocity) with the spatially-resolved susceptibility (slope) and community detection (Porter et al., 2009; Mucha et al., 2010; Fazelpour et al., 2023) to cluster regions that are moving at relatively higher speeds and/or are on steeper slopes. A visual representation of this method is shown in Figure 3 of Desai et al. (2023). Our methods were developed in Desai et al. (2023), and are briefly summarized here (code is available at Desai (2022)).

In the multilayer network, each layer corresponds to an InSAR ~~snapshot~~ image that overlies the network topology; the network topology consists of a static collection of nodes and edges for each sub-region. Each node represents a patch of area, determined using Poisson sampling, and edges connect the nodes via Delaunay triangulation. Velocity and slope maps from InSAR and DEM, respectively, are incorporated into the network as edge weights that change for each layer in the multilayer network.

In prior work, we calculated the average velocity and slope of any two connected nodes and set that as the edge weight. We successfully identified clusters (patches of area) exhibiting similar hillslope movements that are distinct from surrounding areas via a community detection algorithm that uses modularity optimization ~~. This method~~ (Desai et al., 2023). GenLouvain (Mucha et al., 2010; Jeub et al., 2011-19), a modularity optimization algorithm, divides nodes into communities by identifying where the edge weights are stronger within the community than one would expect at random. ~~We implemented this method using NetWiki-GenLouvain (Mucha et al., 2010; Jeub et al., 2011-19), which~~ This algorithm outputs a matrix consisting of the community ID for each node and time pair~~. The~~ ; the community ID is a unique numeric identifier to for each of the different communities across the entire spatiotemporal map (multilayer network). Within this spatiotemporal community map, we identified areas of persistent communities; these communities are an indicator of areas that are strongly connected and have higher-than-average edge weights – velocity and slope – than the rest of the sub-region.

3.2 Community Persistence

To quantify steady communities, we previously developed a measure known as community persistence (Desai et al., 2023). This measures the persistence of the assignment of nodes to communities over time defined as

$$\Pi_t = \frac{1}{N} \sum_c \frac{c_{t-1} \cap c_t}{n_{c,t}}, \tag{1}$$

where N is the total number of nodes in the network, $n_{c,t}$ is the number of nodes in community c at time t, and $c_{t-1} \cap c_t$ is the number of nodes present in community c at both $t, t-1$.

An increase in community persistence within a sub-region indicates that a ~~patch~~ group of nodes is consistently ~~being identified as more similar~~ more strongly connected to each other (measured via edge weight) than to the rest of the network~~. When there is no single patch of area consistently moving at a faster than average rate, *i.e.*~~ , corresponding to localized motion. Conversely, low persistence occurs when no distinct, consistently clustered motion is observed, such as during dry seasons~~, then community persistence is closer to zero. To~~ .

As done in our prior work (Desai et al., 2023), we compare relative changes in Π across the 17 sub-regions ~~, we consider~~ using the Z-score at time t

$$Z_t = \frac{\Pi_t - \bar{\Pi}}{\sigma(\Pi)}. \tag{2}$$

where $\bar{\Pi}$ is the mean persistence over the entire time period, establishing a baseline of the system, and $\sigma(\Pi)$ is its standard deviation. When $Z_t < 0$, community persistence is below average, typically indicating dry conditions with little landslide activity. In the prior analysis of Mud Creek, we observed ~~a~~ that surrounding communities exhibited a drop in persistence, while those within the Mud Creek zone increased in persistence. This led to a statistically significant increase in Z_t, ~~as high as~~ peaking at $Z = 2.5$, followed by a minor decline ~~right before~~ prior to failure. The value at failure remained statistically significant. To ~~quantify this trend amongst~~ extend this analysis to the 17 sub-regions, we identify the ~~increasing segment – the final period of rise~~ final rising segment before the decline ~~– and find~~ and extract the *peak* Z value, which is the maximum Z-score in the identified segment. We use *peak* Z to quantify differences between sub-regions to better classify the ~~slow-moving landslides~~ regions as stable (peak $Z < 2.5$) or ~~vulnerable~~ hazard-prone (peak $Z \geq 2.5$).

3.3 Multivariate Correlation

We characterized active landslides using data on precipitation, deformation, topography, and InSAR coherence. These indicators were used as benchmarks to evaluate the performance of the community detection results. Specifically, we constructed a correlation matrix to assess the relationship between the peak Z-score and the geophysical indicators. For each of the 17 sub-regions, we computed the following seven variables: number of recorded events; mean slope; mean precipitation; mean displacement; maximum displacement; mean InSAR coherence; mean community persistence $\bar{\Pi}$; and peak Z-score. These metrics were used to quantify and compare the classification of hazard-prone regions with observed landslide events.

4 Results

We used a multilayer network combining slope and velocity data spanning from Nov 2015 to ~~Nov~~ Dec 2022 (just before the observed landslide events in Jan 2023 and Mar 2023) to determine the success of evaluating landslide ~~vulnerability~~ hazard via network science techniques. We visualize the evolution of Z_t for each sub-region in Fig. 2. The size of the data points is proportional to Z_t, with larger circles indicating more persistent communities (higher Z-scores). Only points with $Z_t > 0$ are plotted, as negative Z-scores do not signify landslide ~~vulnerability~~hazard. The colors in Fig. 2[a-b] correspond to the 17 sub-regions shown in Fig. 1[a].

Over the period shown, we observe cyclical changes in Z_t corresponding to the wet and dry seasons. Following wet seasons, Z_t is stronger and after dry seasons, Z_t is weaker. Particularly, we observe high Z_t values in fall of 2022; this is because the study area experienced higher than average precipitation that year. The final 100 days of the period (Fig. 2[b]) display differences in Z-scores across the sub-regions, aiding in the identification of potentially stable and ~~vulnerable~~ hazard-prone areas. A clear distinction is made between sub-regions with ~~steadily~~ an increasing Z-scores (outlined in black) and those exhibiting relatively stable Z-scores during those last 100 days.

As previously discussed, a continuous increase in Z-score, like that observed in Mud Creek, indicates ~~vulnerability to landslide events~~high likelihood of a landslide event. To quantify the trends in ~~Fig. 2[b]~~Fig. 2[a-b], we identify the peak Z of the final continuously increasing segment ~~in Fig. 2[c]. Here, darker~~ and plot the values in Fig. 2[c], where sub-regions ~~represent higher peak Z-scores.~~ $Z < 2.5$ are blue and sub-regions ~~with a relatively stable Z-score had peak $Z < 2.5$. Within the sub-regions that showed increasing Z, some sub-regions have peak $Z < 3$, and some have peak $Z \geq 2.5$. Those sub-regions with peak $Z \geq 2.5$ are asterisked in Fig. 2[b]; these sub-regions displayed a steady increase in Z_t and experienced a landslide event soon after Dec 2022.~~ $Z \geq 2.5$ are red. The landslide events are plotted as white dots with images taken by California Transit Authority (Drabinski and Bertola, 2023a, b, c) included in Fig. 2[c]. All dots representing landslide events appear in red regions. Sub-regions with a relatively stable Z-score had peak $Z < 2.5$. The sub-regions that had an increasing Z-score in Fig. 2[b] and peak $Z < 2.5$ did not experience a landslide event. All sub-regions with peak $Z \geq 2.5$ and a steady increase in Z_t experienced a landslide event soon after Dec 2022, initialed in Fig. 2[b].

~~Analysis after the January landslide events (Nov 2015 to Feb 2023) (shown in Supporting Information S1) shows the peak Z-score decreasing for the sub-region containing Paul's Slide. In addition, the Z-score of the sub-region containing Dani Creek Slide is steadily increasing, leading up to its landslide event on 12 Mar 2023 with a peak Z is 2.87, which falls under the classification of *vulnerable*. Gilbert's Slide experienced its landslide event on 16 Mar 2023, but the peak $Z = 1$, which falls as a *stable* region and is falsely classified. The rest of the sub-regions are classified as stable.~~

4.1 Multivariate Analysis

We used a multivariate analysis to compare the traits of the active landslides using ~~information about~~ precipitation, deformation, topography, and radar coherence ~~,~~ with the results of community detection. Fig. 3 ~~visualizes~~ presents the correlation matrix between seven variables for the 17 sub-regions: number of recorded events; mean slope; mean precipitation; mean dis-

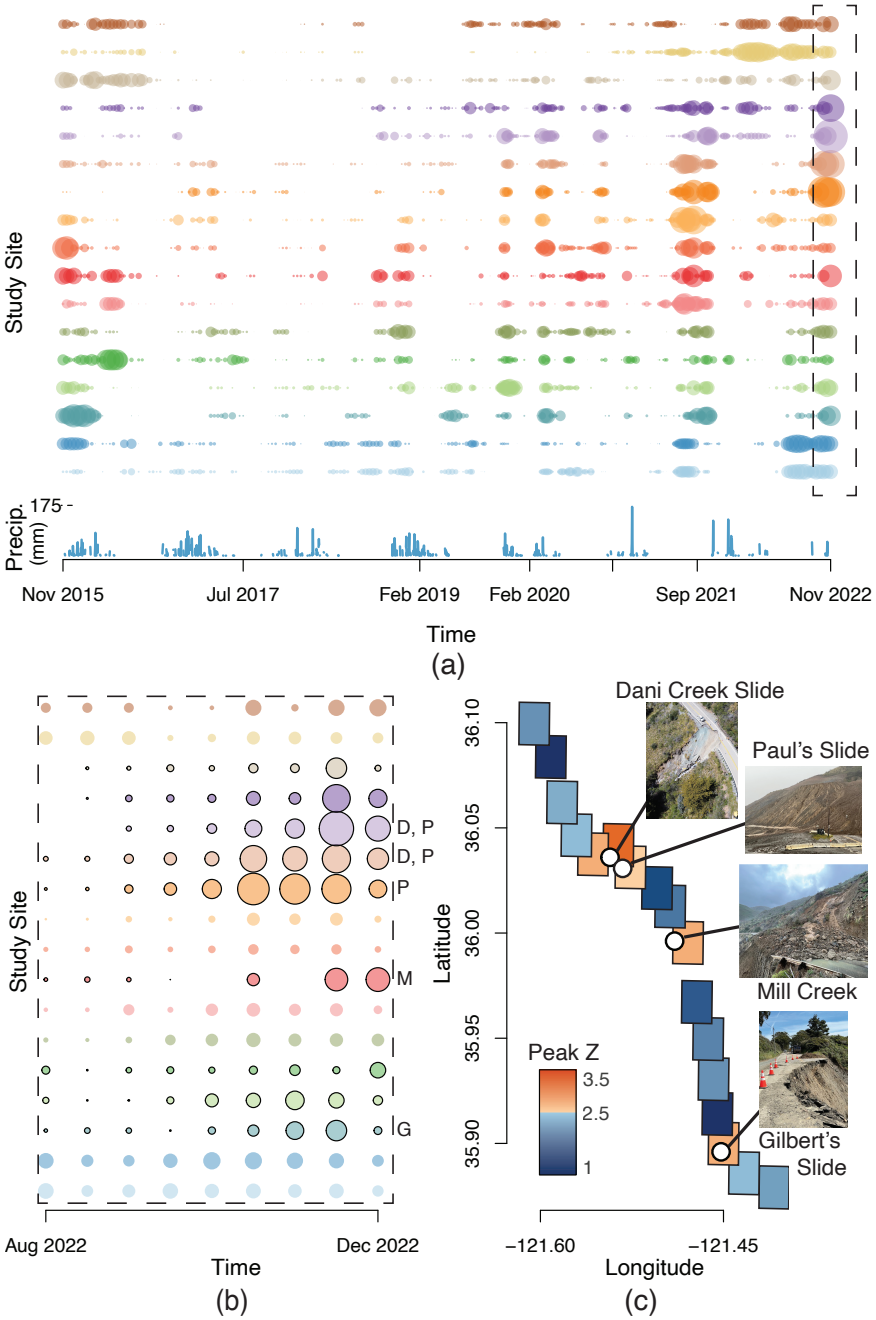

Figure 2. Z-score for community persistence. (a) The Z-score for community persistence Z_{Π_t} for a multilayer network containing information from Nov 2015 to Dec 2022. Each color represents a sub-region. The size of the points corresponds to Z_t, where the thicker the point, the higher the Z-score. ~~On the bottom, the time~~ (b) Time from Aug 2022 to Dec 2022 is shown (inset from [a]), ~~as well as the~~ where regions with a continuous increasing segment are outlined in black. (c) Spatial plot of peak Z-score~~is plotted on the right~~, with regions colored from blue to red. The landslide events that occurred in W22-3 are ~~shown as asterisks~~ initialed in [b] and shown as white dots in [c] , with the corresponding images taken by ~~Caltrans~~ CalTrans (Drabinski and Bertola, 2023a, b, c).

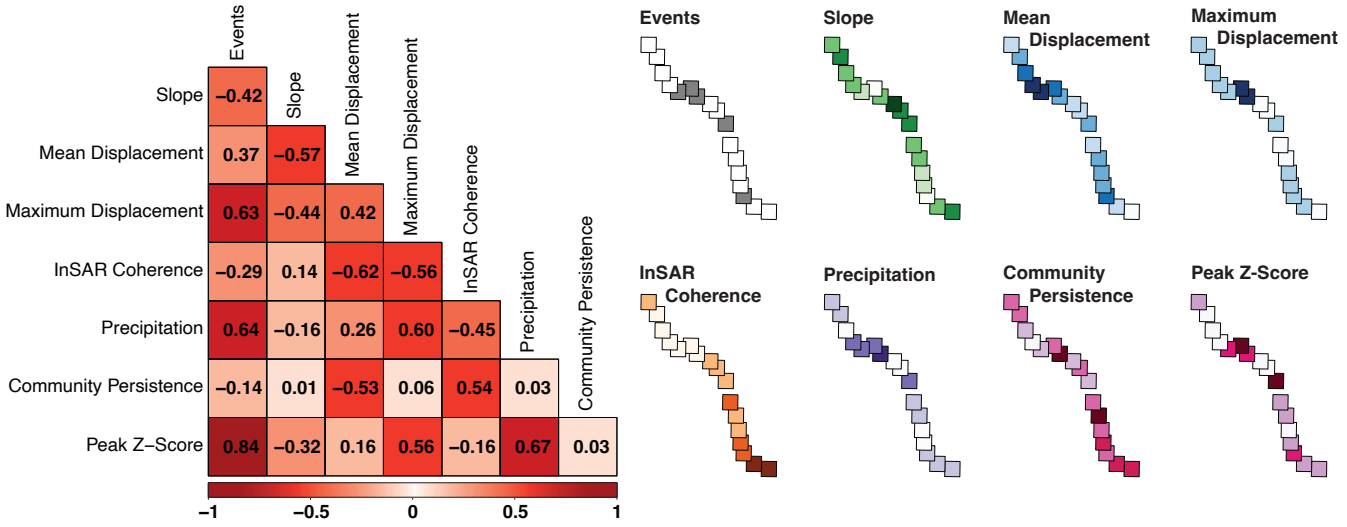

Figure 3. Correlation of Landslide Variables. Correlation for mean precipitation, mean displacement, maximum displacement, mean slope, mean coherence, mean community persistence, peak Z-score of community persistence, and number of events. ~~Each variable is~~ Variables are scaled from minimum to maximum~~and plotted for the 17 sub-regions where a~~ , with darker ~~color means a~~ colors indicating higher ~~magnitude~~values.

placement; maximum displacement; mean InSAR coherence; mean community persistence $\bar{\Pi}$; and peak Z-score~~for each of the 17 sub-regions~~. The spatial distribution for each of the variables is shown in Fig. 3, where the variables are scaled from minimum to maximum and darker color indicates a higher magnitude.

Peak Z-score is positively correlated with recorded events (0.84). Community persistence exhibits ~~positive~~ moderate correlations with mean displacement (-0.53), and InSAR coherence (0.54). ~~Peak Z-score shows strong correlations with recorded events (0.84), maximum displacement (0.56), and precipitation (0.67). Mean displacement demonstrates strong~~ Mean displacement shows negative correlations with slope (-0.57) and InSAR coherence (-0.62), while maximum displacement is ~~strongly correlated~~ correlated positively with precipitation (0.60), ~~InSAR coherence (-0.56), and events (0.63~~recorded events (0.63), peak Z-score (0.56), and negatively with InSAR coherence (-0.56). Moreover, precipitation has a strong positive correlation ~~by 0.63 with precipitation~~with recorded events (0.63) and peak Z-score (0.67).

~~The correlations observed for~~

5 Discussion

Through the integration of network science techniques, remote sensing data, and multivariate analysis, this study identifies several key insights into the detection and characterization of landslide-prone regions. The results highlight the promise of

the peak Z ~~and $\bar{\Pi}$ highlight distinct relationships with~~ -score as a method for early detection and classification of hazardous sub-regions. Because the analysis was conducted within a single geographic region and based on a limited number of documented landslide events, the outcomes presented here should be viewed as a demonstration of potential rather than a definitive or universally generalizable result. Further validation across different terrains, climates, and geologic settings will be essential to establish the broader applicability of this approach as a monitoring tool.

5.1 Spatial Scale

Our analysis was conducted at a subregional scale of 5 km^2, larger than typical landslide areas of a few 0.1 km^2, in order to incorporate a mix of stable and unstable terrain within each subregion. Such variation is critical for the modularity optimization algorithm to identify clustered anomalous behavior. The presence of stable hillslopes provides a baseline against which unstable slopes transitioning to catastrophic failure can be detected as outliers, given that nearby hillslopes experience similar weather conditions. Reducing the size of the subregion would limit the amount of stable terrain, undermining the algorithm's ability to detect relative deviations. Conversely, increasing the spatial extent would significantly raise computational demands without improving performance or sensitivity. This trade-off between spatial scale and computational efficiency is especially important when identifying early signals of slope reorganization that precede catastrophic failure. A potential direction for future work is to assess whether applying this method at smaller spatial scales could improve the model's performance. While such an approach might enhance its utility for real-time landslide monitoring, it would also reduce terrain heterogeneity, potentially diminishing the algorithm's capacity to distinguish anomalous behavior. If this method were to be operationalized as a monitoring tool, a detailed investigation of how terrain uniformity and subregion size affect performance would be essential.

5.2 Comparison of Network-Based Metrics and Geophysical Indicators

The correlation analysis highlights important relationships between geophysical variables, network-based metrics, and precipitation-induced ~~slow-moving landslides. The strong correlation between~~ landslide activity. Notably, the peak Z-score shows a strong positive correlation with recorded landslide events, maximum displacement, and precipitation. This suggests that peak Z ~~suggest that community detection captures~~ is an effective proxy for capturing patterns indicative of an increased potential ~~of landslide events.~~ for landslide events, particularly in response to seasonal hydrologic forcing.

Conversely, the negative correlation between ~~maximum and mean displacement values and coherence suggest~~ both mean and max displacement and InSAR coherence supports previous findings that landslides moving rapidly ~~are eluding~~ often evade detection by InSAR (Yunjun et al., 2019). ~~Despite~~ Although slope exhibits a weak relationship with $\bar{\Pi}$, ~~slope exhibits~~ it shows a strong correlation with mean displacement~~, implying~~ . This indicates that the multilayer network is not biased towards steep slopes but rather amplifies steeper hillslopes ~~with higher deformation. Furthermore, the strong relationship between displacement, $\bar{\Pi}$, and precipitation indicates that community persistence factors in precipitation without requiring additional hydrological modeling~~undergoing deformation. Collectively, these findings demonstrate that network-based metrics – community persistence and peak Z – not only align with traditional indicators of landslide hazard but additionally captures evolving structural patterns in hillslope dynamics which improve classification of hillslopes as hazardous.

~~Several~~ Furthermore, several distinct features emerge when comparing the spatial variability along the eight coastline graphs in Fig. 3. Both mean and maximum displacement ~~strongly~~ prominently highlight the sub-region containing Paul's Slide and Dani Creek Slide~~, but~~ . However, notable differences exist throughout the rest of the study area. ~~These differences occur because calculating the mean suppresses signals of instability~~ While measuring mean displacement tends to smooth over localized or sudden deformation and instead emphasizes areas with multiple slow-moving landslides~~. Conversely, using the~~ , maximum displacement highlights ~~sub-regions with large deformation or high instability, correlating to areas more vulnerable to landslide events. The peak~~ acute deformation signaling higher instability. Peak Z ~~-score and maximum displacement underscore~~ similarly emphasizes Paul's Slide as a ~~significant area of concern for potential landslide events, a fact~~ high-risk region – validated by a major slip off Highway 1 at Paul's Slide in Jan 2023, occurring just a month after ~~this analysis~~ the analysis period.

~~While~~ Despite both maximum displacement and peak Z-score ~~highlight~~ highlighting Paul's Slide, differences between the two variables ~~remain. For instance, the~~ is evident in other sub-regions. Some sub-regions with the highest peak Z-score ~~are not the same as those with the most displacement. Additionally,~~ do not exhibit the greatest displacement, and sub-regions with similar ~~maximum displacement show a~~ displacement magnitudes show a wide range of peak ~~Z-score values, suggesting~~ Z-scores. These discrepancies suggest that community detection ~~results~~ is capturing additional mesoscale dynamics, such as localized shifts in slope behavior or evolving stability, that are not solely influenced by landslide deformation or slope susceptibility~~, but also by meso-scale information that enhances their reliability. Temporal patterns identified through velocity analysis capture nuances~~ .

While the volume removed in Paul's Slide is much larger than for the other landslide events, the initial surface area of motion is comparable to the three other landslides. The signal detected by the network method arises from a combination of dynamic surface factors, not the eventual scale of failure. Since our analysis is based solely on surface movement, the volume ultimately displaced during a landslide is not an input for our calculations—underscoring that our method captures precursory surface behavior rather than relying on post-event consequences.

This reinforces the value of network-based methods in revealing nuanced temporal patterns and transitions that would otherwise remain ~~undetected if these variablesare considered in isolation.~~ hidden when relying solely on conventional geophysical variables.

5.3 Hydrologic Integration

To evaluate whether hydrological forcing could improve community detection outcomes, we incorporated precipitation data from PRISM (Oregon State Univeristy, 2015) in combination with velocity and slope (see Appendix A). However, no notable changes were observed in the community detection results. This lack of sensitivity may stem from the low resolution of PRISM grids, as well as limited data availability near the coasts, potentially rendering the changes too coarse for the community detection algorithm to detect.

To further test this hypothesis, we repeated the experiment using high-resolution precipitation input from a WRF-Hydro model (Li et al., 2023). Even with this improved spatial resolution, there was little improvement in the analysis. The strong correlation (0.67) between peak Z and precipitation data (see Fig. 3) suggests that community detection metrics already

captures underlying hydrological mechanisms, or at least the surface hydrology, and therefore makes the inclusion of precipitation redundant. Advancements in in-situ soil moisture measurements could further improve the applicability of hydrological models, particularly for deep-seated landslide studies.

6 Conclusions

The extension of network science techniques from the Mud Creek case study to the broader Big Sur region yielded promising results. By subdividing the region into smaller sub-regions for varied terrain, we tested the effectiveness of this method as a monitoring technique. The outcomes of community detection served as robust indicators of the landslide events in ~~W22-3~~W22-23, as seen in Fig. 2. Notably, the steady increase in Z_t leading up to failure~~emerged as a crucial indicator~~, alongside the magnitude of Z_t, emerged as a crucial indicator. For instance, Paul's Slide exemplifies how outliers in Z_t can serve as early indicators of ~~vulnerability to~~ increased likelihood of landslide events. Had this analysis been conducted in the relevant time frame, Paul's Slide, alongside Mill's Creek, Dani Creek Slide, and Gilbert's Slide, could have been identified as areas of concern, potentially allowing for preemptive monitoring and mitigation measures.

~~When evaluating the model's performance in classifying sub-regions as stable or vulnerable, we analyzed two time periods: Nov 2015 to Nov 2022 and Nov 2015 to Feb 2023. In the shorter period analysis, all five sub-regions that experienced a landslide event in either Jan or Mar 2023 were correctly classified as vulnerable, and the other twelve sub-regions were accurately identified as stable. In the longer period analysis, there are two sub-regions that experienced a landslide event in Mar 2023. Only one of the two sub-regions was classified as vulnerable, while the other sub-region was incorrectly classified as stable; the remaining fifteen were correctly classified as stable. Consequently, the peak Z-score method achieved a 97% success rate in classifying sub-regions as either stable or vulnerable, with Gilbert's Slide being incorrectly classified as stable in the Nov 2015 to Feb 2023 analysis. It is important to note that these results are based on a limited dataset, which may introduce some bias in the evaluation of the model's performance. As such, the 97% success rate should be interpreted with caution, as it reflects the model's performance within this specific region and time rather than a generalized outcome.~~

~~Comparing~~ Our comparison of landslide susceptibility factors – landslide inventory, slope, cumulative displacement, precipitation, and InSAR coherence – with the outcomes of community detection, peak Z-score, underscores the importance of integrating multiple data sources. Each factor taken alone does not yield enough information to predict landslide~~vulnerability~~, highlighting the need for comprehensive analyses. Furthermore, incorporating the entire temporal period captured by InSAR into the multilayer network improved classification between stable and ~~vulnerable slow-moving landslides~~hazard-prone sub-regions. However, it is crucial to ensure that remote sensing data accurately capture ground surface deformation for statistical analyses to be reliable.

~~In an effort to enhance our results, we combine precipitation data from PRISM (Oregon State Univeristy, 2015) with~~ Overall, the physically informed framework developed here—relying on measured creep velocity and slope~~in S2. However, no changes were observed in the community detection results. This lack of change may be attributed to the low resolution of PRISM grids and the lack of data near the coasts potentially rendering the changes too coarse for the community detection algorithm to detect.~~

~~Subsequently, experiments with high-resolution datasets, such as those obtained from a WRF-Hydro model (Li et al., 2023), also yielded no improvements in the analysis. The strong correlation (−80%) between displacement and precipitation data suggests that velocity data adequately captures underlying hydrological mechanisms, or at least surface hydrology, and therefore makes the inclusion of precipitation redundant. Advancements in in-situ soil moisture measurements could further improve the applicability of hydrological models, particularly for deep-seated landslide studies.~~ —demonstrated strong potential for enhancing landslide hazard assessment. In particular, network metrics such as the peak Z -score offered a sensitive and scalable means of identifying emerging instability, even prior to failure. These findings support the utility of community detection techniques as a complement to conventional geophysical indicators, paving the way for improved, near real-time monitoring systems that can generate dynamic hazard maps and inform timely risk management strategies.

~~Through the methods employed in this study, we identified areas that exhibit a heightened probability of experiencing a landslide event. As such, a physically informed framework relying solely on measured creep velocity and slope yielded highly promising outcomes. These findings hold the potential to significantly enhance monitoring efforts.~~

Code and data availability. The extents of the sub-regions are archived on DataDryad (Desai et al., 2024). Copernicus DEMs are available at https://spacedata.copernicus.eu/collections/copernicus-digital-elevation-model. On-Demand InSAR products were downloaded via Alaska Satellite Facility's HyP3 platform, availabe at https://hyp3-docs.asf.alaska.edu. Sentinel-1 data are available at https://search.asf.alaska.edu/, the ASF data search vertex. The full list of interferograms used are archived on DataDryad (Desai et al., 2024). The Miami INsar Time-Series software in PYthon (MintPy) is available at https://github.com/insarlab/MintPy. Precipitation data is provided by Parameter-elevation Regressions on Independent Slopes Model (PRISM) and is available at https://prism.oregonstate.edu/. Daily precipitation time series is taken for each of the sub-regions. The code used for creating the multilayer networks is available at https://github.com/vddesai-97/networkLandslide, and running the community detection algorithm is on https://github.com/GenLouvain/GenLouvain. The multilayer networks (nodes, edges, weights) for each of the sub-regions are archived on DataDryad (Desai et al., 2024).

Appendix A: Inclusion of hydrological information into the multilayer network

Landslide studies often use precipitation data from (1) site-specific rain gauges with limited spatial coverage and nonuniform temporal resolution, or (2) spatially continuous interpolated gridded rain data. Effective and efficient monitoring of hydrological data has not yet caught up with remote sensing technology to produce high spatial and temporal datasets. Satellite-derived data, such as Soil Moisture Active Passive maps, which use passive microwave techniques and remotely sensed surface soil moisture on a global scale, underestimates in heavily vegetated areas (Das et al., 2019; Reichle et al., 2017; Fan et al., 2020). Remote sensing techniques only detect surface-level soil moisture, and process-based land surface models typically extend the soil moisture estimates to one to two meters below the ground surface but have low spatial resolution (Koster et al., 2009). Therefore, we consider two hydrological datasets: PRISM (Parameter-elevation Relationships on Independent Slopes Model) for precipitation and WRF-Hydro (Weather Research and Forecasting Hydrological modeling framework) for soil moisture and precipitation on the Big Sur Coast.

PRISM The PRISM Climate Group develops spatial climate datasets using various monitoring networks and modeling techniques (Daly et al., 2008). These datasets include daily, monthly, and annual precipitation, and minimum and maximum temperatures for the contiguous United States. PRISM interpolates station measurements using a climate-elevation regression model that considers factors such as coastal distance, topography, and atmospheric conditions. There are about 13,000 stations that collect precipitation data and 10,000 for temperature. PRISM datasets have shown improved results for mountainous and coastal regions of the western United States, including our study sites.

WRF-Hydro WRF-Hydro is an open-source, physics-informed hydrological model (Gochis and Barlage, 2020). The model disaggregates precipitation at the land surface and simulates landslide-relevant processes such as water table depth, infiltration, subsurface lateral flow, and soil moisture using information like soil type, topography, and antecedent conditions. Li et al. (2023) utilized WRF-Hydro to simulate soil moisture within the Big Sur Coast region, incorporating seven in-situ soil moisture stations and nine USGS stream gages. This region has a complex terrain with heterogeneous vegetation, elevation, and slope. The data used in this study has a default soil column with a depth of 2 meters, divided into four layers: 0-10 cm, 10-40 cm, 40-100 cm, and 100-200 cm. Li et al. (2023) demonstrated that WRF-Hydro outperforms many established soil moisture products through data-informed methods that improve soil parameters.

The two datasets differ in resolution and the type of hydrological forcing they represent. PRISM has a 4 km^2 resolution with daily precipitation outputs in mm, while WRF-Hydro has a 1 km^2 resolution with outputs of soil moisture at different depths.

We considered soil moisture, water table depth, and precipitation as additional information to incorporate into the multilayer network as weights in addition to velocity and slope. There was insufficient difference in the community persistence signal when including hydrological information of any type. This is likely because velocity already incorporates underlying hydrological mechanics. When there is enough water in the soil, frictional resistance reduces, causing slow-moving hillslopes to speed up. As the soil dries, the hillslopes slow down. Since this information is already included in the multilayer network, adding hydrology data is redundant. Another reason the hydrology data might not be useful is that Mud Creek is a deep-seated landslide, and the data only went to 200 cm below the surface. To test the effects of adding in hydrological information on the community persistence of the 17 study sites, we applied precipitation data from PRISM (chosen for its success in the Western U.S.) as one of the weights, along with velocity and slope, for the multilayer network. Fig. A1 shows the mean community persistence Π, as discussed in the paper. The results for the multilayer network with weights $w = vs$, where v is velocity and s is slope, is shown in Fig. A1[a] and Fig. A1[b] shows the results for weights $w = vsp$, where p is precipitation from PRISM. We observe that including precipitation as a weight shows minimal differences in the community detection.

~~Z-score for community persistence.The Z-score for community persistence Z_{Π_t} for a multilayer network containing information from Nov 2015 to Feb 2023. Each color represents a sub-region. The thickness of the points corresponds to Z_t, where the thicker the point, the higher the Z-score. On the bottom, the time from Aug 2022 to Feb 2023 is shown, as well as the peak Z-score is plotted on the right. The landslide events that occurred in Mar 2023 are shown as asterisks in band white dots in c, with the corresponding images taken by Caltrans (Drabinski and Bertola, 2023a, b, c).~~

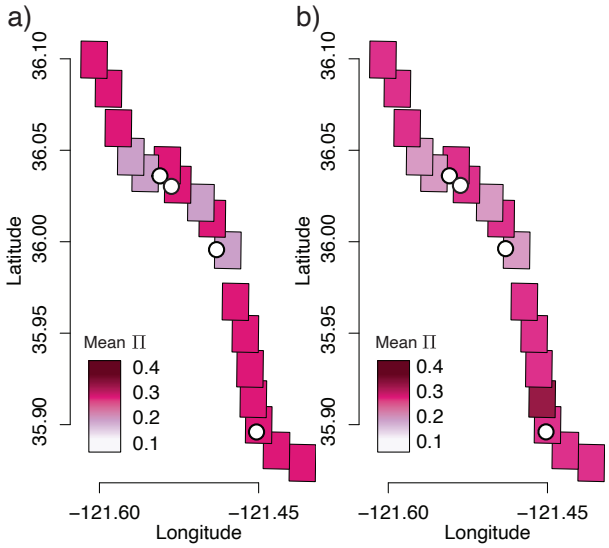

Figure A1. Geographical distribution of Z-scores. ~~Max~~ Mean Z-Score for [a] weights $w = vs$ compared against [b] weights $w = vsp$. The white dots are the landslide events.

Author contributions. VDD developed and carried out the analysis, and KED and ALH assisted throughout the development and analysis. ALH prepared the InSAR data. VDD prepared the paper and figures, and ALH and KED provided comments and edits.

Competing interests. The contact author has declared that none of the authors has any competing interests.

Acknowledgements. This work was supported by NSF grant PREEVENTS ICER-1854977 and we are grateful for conversations with our collaborators on ~~that project~~this project. We also acknowledge the WRF-Hydro analysis conducted under this grant by Chuxuan Li and Daniel E. Horton, the results of which were used in Appendix A. Part of this research was carried out at the Jet Propulsion Laboratory, California Institute of Technology, under a contract with the National Aeronautics and Space Administration (80NM0018D0004), and supported by the Earth Surface and Interior program.

References

Barrat, A., Barthélemy, M., and Vespignani, A.: Dynamical Processes on Complex Networks, Cambridge University Press, 1st edn., ISBN 9780521879507 9780511791383 9781107626256, https://doi.org/10.1017/CBO9780511791383, 2008.

Bassett, D. S., Wymbs, N. F., Porter, M. A., Mucha, P. J., Carlson, J. M., and Grafton, S. T.: Dynamic reconfiguration of human brain networks during learning, Proceedings of the National Academy of Sciences, 108, 7641–7646, https://doi.org/10.1073/pnas.1018985108, 2011.

Bennett, G. L., Roering, J. J., Mackey, B. H., Handwerger, A. L., Schmidt, D. A., and Guillod, B. P.: Historic drought puts the brakes on earthflows in Northern California, Geophysical Research Letters, 43, 5725–5731, https://doi.org/10.1002/2016GL068378, 2016.

Berthier, E., Porter, M. A., and Daniels, K. E.: Forecasting failure locations in two-dimensional disordered lattices, Proceedings of the National Academy of Sciences, 116, 16 742–16 749, https://doi.org/10.1073/pnas.1900272116, 2019.

Booth, A. M., McCarley, J. C., and Nelson, J.: Multi-year, three-dimensional landslide surface deformation from repeat lidar and response to precipitation: Mill Gulch earthflow, California, Landslides, 17, 1283–1296, https://doi.org/10.1007/s10346-020-01364-z, 2020.

California Department of Conservation: Reported California Landslides, https://www.conservation.ca.gov/cgs/landslides, 2023.

Copernicus: Copernicus Digital Elevation Model, https://doi.org/10.5270/ESA-c5d3d65, accessed on 2023-07-20, 2021.

Daly, C., Halbleib, M., Smith, J. I., Gibson, W. P., Doggett, M. K., Taylor, G. H., Curtis, J., and Pasteris, P. P.: Physiographically sensitive mapping of climatological temperature and precipitation across the conterminous United States, International Journal of Climatology, 28, 2031–2064, https://doi.org/10.1002/joc.1688, 2008.

Das, N. N., Entekhabi, D., Dunbar, R. S., Chaubell, M. J., Colliander, A., Yueh, S., Jagdhuber, T., Chen, F., Crow, W., O'Neill, P. E., Walker, J. P., Berg, A., Bosch, D. D., Caldwell, T., Cosh, M. H., Collins, C. H., Lopez-Baeza, E., and Thibeault, M.: The SMAP and Copernicus Sentinel 1A/B microwave active-passive high resolution surface soil moisture product, Remote Sensing of Environment, 233, 111 380, https://doi.org/10.1016/j.rse.2019.111380, 2019.

Desai, V. D.: networkLandslide, http://github.com/vddesai-97/networkLandslide, 2022.

Desai, V. D., Fazelpour, F., Handwerger, A. L., and Daniels, K. E.: Forecasting landslides using community detection on geophysical satellite data, Physical Review E, 108, 014 901, https://doi.org/10.1103/PhysRevE.108.014901, 2023.

Desai, V. D., Handwerger, A. L., and Daniels, K. E.: Data from: Using Network Science to Evaluate Vulnerability of Landslides on Big Sur Coast, California, USA [Dataset], https://doi.org/10.5061/dryad.1jwstqk42, 2024.

Drabinski, K. and Bertola, A.: Update25, California Transportation, https://blogbigsur.wordpress.com/2023/03/07/highway-1-at-mill-creek-to-open-by-end-of-march-pauls-slide-still-set-for-long-term-closure/, 2023a.

Drabinski, K. and Bertola, A.: Update31, California Transportation, https://blogbigsur.wordpress.com/2023/03/16/update-31-assessments-on-highway-1-continue-at-areas-damaged-by-most-recent-storms/, 2023b.

Drabinski, K. and Bertola, A.: Update37, California Transportation, https://blogbigsur.wordpress.com/2023/03/31/update-37-with-repairs-underway-travel-opportunites-still-abound-on-the-big-sur-coast/, 2023c.

Fan, X., Liu, Y., Gan, G., and Wu, G.: SMAP underestimates soil moisture in vegetation-disturbed areas primarily as a result of biased surface temperature data, Remote Sensing of Environment, 247, 111 914, https://doi.org/10.1016/j.rse.2020.111914, 2020.

Fazelpour, F., Desai, V. D., and Daniels, K. E.: Community detection forecasts material failure in a sheared granular material, https://doi.org/10.48550/arXiv.2307.07501, arXiv:2307.07501 [cond-mat], 2023.

Fletcher, K., European Space Agency, and European Space Research and Technology Centre, eds.: InSAR principles: guidelines for SAR interferometry processing and interpretation, no. 19 in ESA TM, ESA Publications, ESTEC, Noordwijk, the Netherlands, ISBN 9789290922339, oCLC: 137242934, 2007.

Glastonbury, J. and Fell, R.: Geotechnical characteristics of large slow, very slow, and extremely slow landslides, Canadian Geotechnical Journal, 45, 984–1005, https://doi.org/10.1139/T08-021, 2008.

Gochis, D. and Barlage, M.: WRF-Hydro® Modeling System | Research Applications Laboratory, https://ral.ucar.edu/projects/wrf_hydro, https://ral.ucar.edu/projects/wrf_hydro, 2020.

Handwerger, A. L., Fielding, E. J., Huang, M., Bennett, G. L., Liang, C., and Schulz, W. H.: Widespread Initiation, Reactivation, and Acceleration of Landslides in the Northern California Coast Ranges due to Extreme Rainfall, Journal of Geophysical Research: Earth Surface, 124, 1782–1797, https://doi.org/10.1029/2019JF005035, 2019.

Handwerger, A. L., Fielding, E. J., Sangha, S. S., and Bekaert, D. P. S.: Landslide Sensitivity and Response to Precipitation Changes in Wet and Dry Climates, Geophysical Research Letters, 49, https://doi.org/10.1029/2022GL099499, 2022.

Hogenson, K., Kristenson, H., Kennedy, J., Johnston, A., Rine, J., Logan, T., Zhu, J., Williams, F., Herrmann, J., Smale, J., , and Meyer, F.: Hybrid Pluggable Processing Pipeline (HyP3): A cloud-native infrastructure for generic processing of SAR data [Computer software], https://doi.org/10.5281/zenodo.4646138, 2020.

Hungr, O., Leroueil, S., and Picarelli, L.: The Varnes classification of landslide types, an update, Landslides, 11, 167–194, https://doi.org/10.1007/s10346-013-0436-y, 2014.

Jeub, L. G. S., Bazzi, M., Jutla, I. S., and Mucha, P. J.: A generalized Louvain method for community detection implemented in MATLAB, http://netwiki.amath.unc.edu/GenLouvain, https://github.com/GenLouvain/GenLouvain/tags, downloaded on 2020-05-15, 2011-19.

Jones, E. S., Mirus, B. B., Schmitt, R. G., Baum, R. L., Godt, J. W., Kirschbaum, D. B., Stanley, T. A., and MCCoy, K. E.: Summary Metadata - Landslide Inventories across the United States, https://doi.org/10.5066/P9E2A37P, 2019.

Kirschbaum, D., Kapnick, S. B., Stanley, T., and Pascale, S.: Changes in Extreme Precipitation and Landslides Over High Mountain Asia, Geophysical Research Letters, 47, e2019GL085 347, https://doi.org/10.1029/2019GL085347, 2020.

Kivela, M., Arenas, A., Barthelemy, M., Gleeson, J. P., Moreno, Y., and Porter, M. A.: Multilayer networks, Journal of Complex Networks, 2, 203–271, https://doi.org/10.1093/comnet/cnu016, 2014.

Koster, R. D., Guo, Z., Yang, R., Dirmeyer, P. A., Mitchell, K., and Puma, M. J.: On the Nature of Soil Moisture in Land Surface Models, Journal of Climate, 22, 4322–4335, https://doi.org/10.1175/2009JCLI2832.1, 2009.

Lacroix, P., Handwerger, A. L., and Bièvre, G.: Life and death of slow-moving landslides, Nature Reviews Earth & Environment, 1, 404–419, https://doi.org/10.1038/s43017-020-0072-8, 2020.

Li, C., Yu, G., Wang, J., and Horton, D. E.: Toward improved regional hydrological model performance using state-of-the-science data-informed soil parameters, Water Resources Research, https://doi.org/10.1029/2023WR034431, 2023.

Mucha, P., Richardson, T., Macon, K., Porter, M., and Onnela, J.-P.: Community Structure in Time-Dependent, Multiscale, and Multiplex Networks, Science, 328, 876–878, http://www.jstor.org/stable/40655926, 2010.

Nabizadeh, M., Singh, A., and Jamali, S.: Structure and Dynamics of Force Clusters and Networks in Shear Thickening Suspensions, Physical Review Letters, 129, 068 001, https://doi.org/10.1103/PhysRevLett.129.068001, publisher: American Physical Society, 2022.

Newman, M. E. J.: Networks: an introduction, Oxford University Press, Oxford; New York, ISBN 978-0-19-920665-0, 2010.

Nguyen, C., Peetz, D., Elbanna, A. E., and Carlson, J. M.: Characterization of fracture in topology-optimized bioinspired networks, Physical Review E, 100, 042 402, https://doi.org/10.1103/PhysRevE.100.042402, 2019.

Oregon State Univeristy: PRISM Climate Group, accessed on 2022-01-13. http://prism.oregonstate.edu/, 2015.

Palmer, J.: Creeping earth could hold secret to deadly landslides, Nature, 548, 384–386, https://doi.org/10.1038/548384a, 2017.

Papadopoulos, L., Puckett, J. G., Daniels, K. E., and Bassett, D. S.: Evolution of network architecture in a granular material under compression, Physical Review E, 94, 032 908, https://doi.org/10.1103/PhysRevE.94.032908, 2016.

Porter, M. A. and Gleeson, J. P.: Dynamical Systems on Networks: A Tutorial, vol. 4 of *Frontiers in Applied Dynamical Systems: Reviews and Tutorials*, Springer International Publishing, Cham, ISBN 978-3-319-26640-4 978-3-319-26641-1, https://doi.org/10.1007/978-3-319-26641-1, 2016.

Porter, M. A., Onnela, J.-P., and Mucha, P. J.: Communities in Networks, Notices of the American Mathematical Society, 56, 1082–1097, 1164–1166, 2009.

Reichle, R. H., Draper, C. S., Liu, Q., Girotto, M., Mahanama, S. P. P., Koster, R. D., and De Lannoy, G. J. M.: Assessment of MERRA-2 Land Surface Hydrology Estimates, Journal of Climate, 30, 2937–2960, https://doi.org/10.1175/JCLI-D-16-0720.1, 2017.

Scheingross, J. S., Minchew, B. M., Mackey, B. H., Simons, M., Lamb, M. P., and Hensley, S.: Fault-zone controls on the spatial distribution of slow-moving landslides, Geological Society of America Bulletin, 125, 473–489, https://doi.org/10.1130/B30719.1, 2013.

Wills, C., Manson, M. W., Brown, K., Davenport, C., and Domrose, C.: Landslides in the Highway 1 Corridor: Geology and Slope Stability along the Big Sur Coast between Point Lobos and San Carpoforo Creek, Monterey and San Luis Obispo Counties, California, Tech. rep., Coast Highway Management Plan, https://www.semanticscholar.org/paper/LANDSLIDES-IN-THE-HIGHWAY-1-CORRIDOR%3A-GEOLOGY-AND-Wills-Manson/e2e86d59abc5aaeb57653fe4bbdd226f9d291149, 2005.

Young, A. P.: Recent deep-seated coastal landsliding at San Onofre State Beach, California, Geomorphology, 228, 200–212, https://doi.org/10.1016/j.geomorph.2014.08.005, 2015.

Yunjun, Z., Fattahi, H., and Amelung, F.: Small baseline InSAR time series analysis: Unwrapping error correction and noise reduction, Computers & Geosciences, 133, 104 331, https://doi.org/10.1016/j.cageo.2019.104331, 2019.